Experimental study of chaotic flow and mixing of Newtonian fluid in a rotating arc-wall mixer

Eliane Younes, Yann Moguen, Kamal El Omari, Teodor Burghelea, Yves Le Guer, Cathy Castelain

Experimental study of chaotic flow and mixing of Newtonian fluid in a rotating arc-wall mixer

Eliane Younes[a], Yann Moguen[b], Kamal El Omari[c], Teodor Burghelea[a], Yves Le Guer[d], Cathy Castelain[a,*]

[a] *Université de Nantes, CNRS, Laboratoire de Thermique et Énergie de Nantes, LTeN, UMR 6607, F-44000 Nantes, France*
[b] *Université de Pau et des Pays de l'Adour, E2S UPPA, SIAME, EA 4581, 64100, Anglet, France*
[c] *PIMENT laboratory, University of Reunion Island, 40 Av. Soweto, 97455, Saint-Pierre, La Réunion, France.*
[d] *Université de Pau et des Pays de l'Adour, E2S UPPA, SIAME, EA 4581, 64000, Pau, France*

Abstract

In order to mix highly viscous fluids with minimal energetic input, a new active in-line mixer has been developed in our previous study (El Omari *et al.*, Phys. Rev. Fluids, 2021 [18]). Based on the principle of mixing by chaotic advection, we present in this paper an experimental characterisation of chaotic mixing of Newtonian fluid flows, at low Reynolds number. First, the flow is characterized using velocity field measurements. Distinct flow topologies are detected in the flow. The trajectories of the fluid particles are computed and show the generation of complex structures in the flow. Residence time distributions reveal that the fluid particles spend more time in the mixer under favorable controlling conditions. Finite size Lyapunov exponents are calculated and indicate that the flow is more chaotic for these conditions. Next, the mixing patterns are visualized and showed that the mixing is more homogeneous under the same favorable conditions for which the fluid particles are sufficiently subjected to the stretching and folding mechanism.

Keywords: Chaotic mixing, active mixer, continuous flow, viscous fluids, PIV, LIF

*Corresponding author
Email address: Cathy.Castelain@univ-nantes.fr (Cathy Castelain)

Nomenclature		
T	Period of rotation of the cylinders	s
x,y	Cartesian coordinates	m
t	Time	s
H	Height of the channel	m
W	Width of the channel	m
L	Length of the channel	m
R	Radius of the cylinders	m
U	Inlet velocity of the flow	m/s
l	Divergence of the fluid particles	m
l_0	Initial divergence	m
l_m	Maximum divergence	m
C^*	Dimensionless concentration field	
I	Grey level	
I_{max}	Maximum grey level	
I_{min}	Minimum grey level	
Abbrevations		
RAW	Rotating arc-wall	
PIV	Particle image velocimetry	
LIF	Laser-induced fluorescence	
FSLE	Finite size Lyapunov exponent	
Re	Reynolds number	
St	Strouhal number	
k	Ratio of the transverse flow velocity to the axial flow velocity	
Supscript		
$\bar{}$	Mean value	
Greek letters		
Ω	Angular speed of the cylinders	rad/s
Ω_0	Amplitude of the angular speed of the cylinders	rad/s
μ	Dynamic viscosity	Pa.s
ρ	Density	kg/m^3
σ	Standard deviation	
λ	Lyapunov exponent	

1. Introduction

Many industries require efficient mixing of highly viscous fluids, such as food, cosmetics, pharmaceutical, oil industries, etc. The global purpose of mixing is to ensure the homogeneity of the final product resulting from two or more fluids initially separated.

A natural mechanism of mixing is molecular diffusion. Molecular diffusion is a random process by which molecules of one species undergo a random motion among molecules of a second species. The kinetics of this phenomenon is quantified by the diffusion coefficient D. The characteristic time required to mix by simple molecular diffusion is $t_D \propto \frac{d^2}{D}$, where d is the characteristic length over which the diffusion is active. In the case of viscous fluids, this mechanism is inefficient. This is simply because the molecular diffusion coefficient D, which is inversely proportional to the viscosity, is very small, and the diffusion time becomes too long for practical purposes.

Therefore, additional physical mechanisms are required to increase the contact surface between the fluid elements in order to achieve efficient mixing within realistic time scales. The technique often used is to generate inertial turbulence [16, 15]. However, the generation of turbulence in viscous fluid flow requires high energy consumption [41, 27], in terms of stirring power for mixing in batch tanks or pumping power for continuous flows. This represents a major drawback for most industries. On the other hand, in some processes, the fluids used are often complex fluids with long molecular chains, which can be unintentionally broken by excessive shear stresses in turbulent flows. Therefore, mixing of pasty materials with minimal energetic input and within realistic time scales is a real challenge.

Chaotic advection is considered the most efficient mechanism for mixing viscous fluids [36, 34, 4]. It is used in many applications in order to intensify mass [43, 12, 48] and/or heat transfer [1, 32, 13, 17]. It consists in generating complex trajectories while being in laminar regime. It is based on stretching and folding of the fluid elements which allow to increase the contact surface between the different species promoting the mixing. In order to generate a chaotic advection regime, the number of degree of freedom of the system should be larger than 2 [38, 9, 33]. Chaotic advection regime can be

generated in two-dimensional time-dependent flows [3, 27, 40] or in three-dimensional stationary [26, 25] or non-stationary [47, 46] flows.

Chaotic advection mixers can be categorized into passive and active mixers. Passive mixing can be achieved by using channels with specific shapes such as curved channels [25, 37, 32, 29] or by inserting obstacles in the flow that induce its perturbation [7, 19, 30, 23]. Active mixers use an external energy source to promote mixing. These external energy sources can be moving agitators [3], pressure disturbances [28], acoustic vibrations [20], etc. An obvious advantage of passive mixers is that they require no external energy, but on the other hand, they offer less control over the mixing level.

Mixers can also be classified into continuous or batch mixers. Continuous mixers offer many advantages over batch mixers, as continuous operations provide high production rates and reduce the operating time by eliminating filling, discharging and cleaning operations between two successive cycles. Continuous mixers currently used in industries are not yet fully optimized, mainly because mixing is performed along the entire length of the channel using moving objects (e.g. screw extruders). When the mixing length becomes longer than necessary, several drawbacks appear: product degradation due to excessive mixing and increase in the price of the final product to compensate for the additional energy consumption.

Given the above mentioned reasons, we proposed in previous study [18, 49] a new continuous active mixer with three rotating cylinders located on the walls. A theoretical study was carried out based on two simple phenomenological arguments, one for folding the fluid elements and the other for mixing by molecular diffusion. This study allowed to estimate the mixing efficiency with two non-dimensional controlling parameters: the Strouhal number based on the axial flow velocity and the period of rotation of the cylinders, and the ratio of the transverse flow velocity to the axial flow velocity. A numerical study was also performed for several Strouhal number and velocity ratio. The mixing efficiency was quantified and the results were in good agreement with the results obtained from the heuristic conditions. The numerical results also revealed the presence of an optimal Strouhal number for which the mixing is the most efficient. Moreover, the numerical simulations showed that, in the cases of good mixing effi-

ciency, chaotic advection is detected in the flow.

The present paper provides a systematic characterization of the chaotic flow and the mixing based on the flow fields and the mixing patterns. This study proposes experimental methods to quantify the chaotic advection mixing.

After validating that the active inline mixer is promising for producing chaotic mixing, the present paper provides an experimental characterization of the chaotic mixing, based on the flow fields and the mixing patterns, using several approaches. The paper is organized as follows. The experimental setup is described in Sec. 2.1. The working fluid and the controlling parameters are presented in Sec. 2.2. The experimental methods are detailed in Sec. 2.3. The flow and the mixing are characterized in Sec. 3. The paper closes with a summary of the main conclusions and several perspectives, Sec. 4.

2. Experiments

2.1. Experimental setup

The Rotating Arc-Wall mixer (RAW mixer) is shown in Fig. 1. It is composed of a main channel made of transparent polymethylmethacrylate (PMMA) walls allowing the visualization of the flow; see Fig. 1(b).

The channel has a main length of L = 8 cm and a rectangular cross-section with a width W = 2 cm and a height H = 4 cm. The active mixing zone consists of three PMMA cylinders with equal radii R = 1 cm. The cylinders are positioned vertically over the entire height of the channel. Their axis of rotation are perpendicular to the horizontal plane of the mixer. The distance between the center of the first cylinder and the inlet of the mixing zone is equal to 2 cm. The distance between the centers of the cylinders located on the same wall is equal to 3 cm. The third cylinder is located on the opposite wall, in the middle of the two opposite cylinders. The protrusion distance of the cylinders in the channel is equal to $\Delta = \frac{W}{6} = 0.33$ cm.

The mixer has two inlets with a diameter of 0.5 cm each, and one outlet with a diameter of 1 cm. Both inputs are positioned at the mid-height of the channel. They feed a nozzle having a length of 2 cm and an angle of convergence of 45°. A removable separation is added between the two fluids to prevent mixing upstream of the inlet

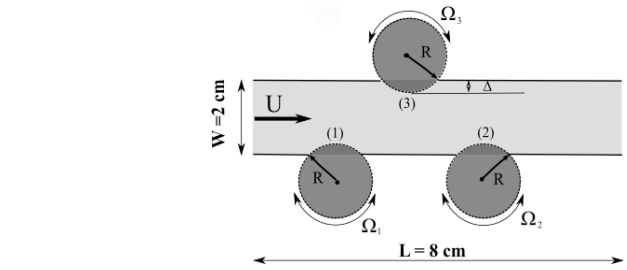

(a)

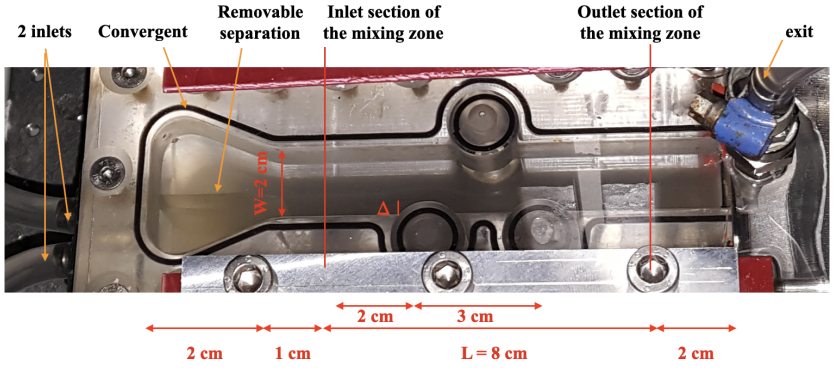

(b)

Figure 1: (a) Sketch of the two-dimensional Rotating Arc-Wall (RAW) mixer, (b) Photo of the RAW mixer.

section of the mixing zone. It is located at half width of the channel; see Fig. 1(b). The outlet is positioned on the top wall to facilitate the total filling of the channel with the fluid.

For laminar flows, the development length L_D of the flow is given by $\frac{L_D}{Dh} \approx 0.06\,Re$ where $D_h = \frac{4A}{P}$ is the hydraulic diameter of the cross-section, and A and P are respectively the area and perimeter of the cross-section. Thus, in order to obtain a fully developed flow at the inlet section of the mixing zone in the studied range of parameters, a section of length 1 cm is added after the nozzle. At the exit of the mixing zone, a section of 2 cm length is added so that the measurements made at the exit of the mixing zone are not affected by back flows. The mixer is machined with a 4-axis milling machine and the cylinders are made using a CNC lathe. The cylinders and the

channel walls are carefully polished to improve their optical transparency and to allow the visualization of the flow.

The fluid supply system consists of two syringe pumps manufactured in-house. To ensure continuous flow for sufficient time, we have designed syringes of 6 cm radius and 40 cm length. Each syringe can contain 4L of fluid. This volume is sufficient for at least one experimental test in the range of parameters we used. High pressures are required to drive viscous fluids at constant flow rate. To achieve this, the flow rate is generated by connecting each piston to a very resistant and high-precision linear actuator (Thomson Linear Motion, Model PC32LX999B04-0400FM1). Given the forces required to move the pistons, a rigid fixation of the entire supply system is necessary. In addition, to ensure a linear and continuous translational movement of the pistons, the assembly required very precise alignment.

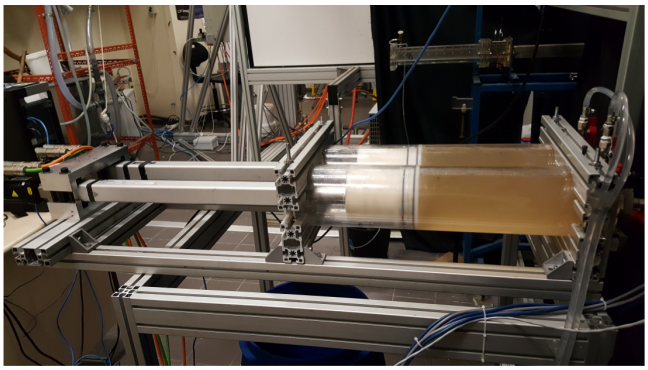

Figure 2: Photo of the syringe pumps.

The rotational protocol of the cylinders is the following: the three cylinders oscillate with the same amplitude Ω_0. The cylinders located on the same wall oscillate in the same direction according to the sine function $\Omega = \Omega_0 \sin\left(\frac{2\pi}{T}t\right)$ and the third cylinder oscillates in the opposite direction $\Omega = -\Omega_0 \sin\left(\frac{2\pi}{T}t\right)$. Here, t is the time and T is the period of rotation of the cylinders. A detailed explanation of the choice of the rotational protocol of the cylinders is given in Ref. [18]. We have shown that the modulation of the angular velocities of the cylinders with a sine function and with opposite directions of rotation generate two flow topologies that alternate smoothly between each other.

Each of the topologies is formed by three elliptical regions. We have also observed the formation of a hyperbolic point beneficial to the mixing. In order to make this hyperbolic point in the middle of the mixing zone we have chosen equal rotational frequencies and velocity amplitudes for the three cylinders. The cylinders are controlled independently by three stepping motors (from National Instruments, Model ST24-E).

2.2. Working fluid and controlling parameters

The Emkarox HV45 (from Croda, France) is the Newtonian fluid used in this study. It is a mixture of polypropylene glycol and polyethylene glycol [2, 8]. It is supplied as a transparent, highly viscous fluid, miscible in water. In an undiluted state, its dynamic viscosity is equal to 100 Pa.s at 20^{o}C. This viscosity is measured using a controlled stress rotational rheometer (Mars III, Thermofischer Scientific). The preparation consists in diluting the right amount of Emkarox in water to reduce its viscosity. The chosen Emkarox solution has a mass concentration of 50% and its dynamic viscosity μ equal to 1.7 Pa.s. The density of the fluid is ρ = 1090.5 kg/m^3, according to the data sheet provided by the supplier. In this study, all experiments were performed with the same inlet velocity U. The corresponding Reynolds number at the inlet of the mixer is equal to Re = $\frac{\rho UW}{\mu}$ = 0.1. The influence of the Reynolds number on the mixing, was studied numerically in Ref. [49]. This study showed that, as long as the inertial effects are negligeable, for Reynolds number below 1, the mixing does not dependent on the Reynolds number.

The previous study, presented in Ref. [18], helped to validate this new mixing concept. It has shown that the non-dimensional numbers that control the flow are: the Strouhal number St = $\frac{W}{TU}$ which represents the ratio of a characteristic time of the flow to the rotational period of the cylinders T, and the velocity ratio k = $\frac{R\Omega_0}{U}$ of the largest angular speed of the cylinders to the axial velocity of the flow.

2.3. Experimental methods

To characterize the flow, two measurement techniques are used: particle image velocimetry (PIV) technique for the velocity field measurements and laser-induced fluorescence (LIF) technique for the visualization of the mixing patterns.

2.3.1. *Optical system and data acquisition*

For both measurement techniques, the same optical system is used. The flow is illuminated by the laser light emitted by a solid state laser (RayPower laser from Dantec Dynamics) with a power P = 5W and a wave length of 514 nm. The primary cylindrical laser beam is split by a beam splitter and each of the two beams is passed through a block of cylindrical optics that converts them in two laser sheets that illuminate the channel at its mid hight and are oriented as schematically illustrated in Fig. 3. The rationale behind using two distinct laser sheets instead of a single one was to minimize the formation of shadowed flow regions which form behind the stirring cylinders. We note that this method only allowed us to increase the light intensity in this zones but did not completely remove the shadows. The flow is visualized from the top by a digital camera (Basler ace USB 3.0 Camera, model acA1920-155um) with a resolution of 1920 pixels $\times$ 1200 pixels equipped with a 35 mm lens (from Edmund Optics). The spatial resolution of the images is 41.67 μm/pixel. The camera is triggered by a real-time controller (cRIO 9045 from National Instruments). The synchronization is made at the beginning of the rotational movement of the cylinders. Once the cylinders start to rotate, the acquisition of images is triggered. By knowing at which time instant an image is taken, we can determine to which moment of the period it corresponds.

2.3.2. *Particle image velocimetry (PIV)*

The fluid is seeded with hollow glass spheres with a diameter of 10 μm (from Dantec Dynamics). In this study, a constant inlet velocity is used for all measurements and a single time step dt = 25 ms between two successive images is considered. It is chosen so that the average displacement of the fluid particles is between 25% and 100% of the size of the smallest interrogation window (16 pixels). Once the images are acquired, they are successively passed through a PIV algorithm (Matlab code) that has been previously developed in-house [50, 44, 39]. The algorithm applies the 2D multigrid cross-correlation method using a sequence of squared interrogation windows with sizes [128, 64, 32, 16] and an overlap of 50%. The instrumental error does not exceed 4 % all over the mixer.

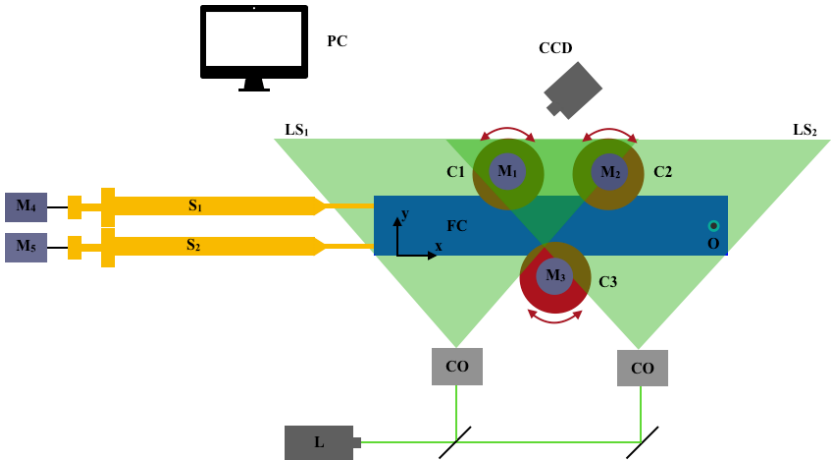

Figure 3: Schematic view of the experimental apparatus: FC- flow channel, S_1, S_2- syringe pumps, O- fluid outlet, C_1, C_2, C_3- cylinders, M_1, M_2, M_3- motors, L- solid state laser, CO- cylindrical optics block, LS_1, LS_2- laser sheets, CCD– digital camera, PC– personal computer. The CCD and the motors are connected to the PC.

2.3.3. Laser-induced fluorescence (LIF)

The dye used for the mixing experiments is the molecular fluorescein. The mixing experiments are performed by uniformly injecting two solutions: a solution with molecular fluorescein and a solution without fluorescein; see Fig. 4. The region illuminated by the laser sheet and containing fluorescein appears bright while the other region without dye is dark. At the beginning of each mixing experiment, each fluid occupies half of the channel. A modification of the interface is observed in the mixing region due to the presence of the static cylinders. The concentration of fluorescein in the dyed solution is equal to C = 0.022 g/L for which the relationship with the light intensity is linear. The exposure time is equal to 6000 µs in order to use the 4096 grey level providing by the 12-bit camera while avoiding saturated areas. For more details, please refer to Ref. [49].

2.3.4. Data analysis

Here, we present the methods we used to calculate the various parameters needed to characterize the chaotic advection regime and the mixing.

In order to identify the stretching and folding process and to highlight the sensitivity

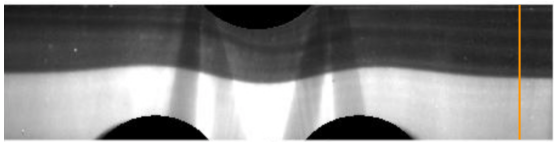

Figure 4: Initial distribution of fluids in the mixer while the cylinders are at rest. The yellow line indicates where the standard deviation $\sigma(C^*)$ of the concentration is evaluated.

of a chaotic system to the initial conditions, the fluid particles can be followed along their trajectories [11, 24, 52, 51]. From the velocity field measurements obtained by the PIV technique, the trajectories of 1000 "virtual" particles uniformly distributed along inlet section of the channel are computed. They are positioned along the inlet section using Matlab. At each time step, the velocity field are interpolated within a 1000×1920 grid using the "griddata" function of Matlab.

At t = 0, all particles are positioned along the inlet section and the cylinders are stationary. Once the cylinders start rotating, the particles move using the corresponding velocity fields $\mathbf{v}(t)$. Each particle has an index. At each time step, the new position of each particle is calculated according to the expression:

$$\mathbf{x}(t+dt) = \mathbf{x}(t) + \mathbf{v}(t)dt. \tag{1}$$

The new positions are then interpolated within the same 1000×1920 grid and the following interpolated velocity field is loaded. This procedure is repeated until all particles exit the channel. By knowing the index of each particle and the position of the indexed particle at each time step, we can plot the trajectory of any desired particle.

In continuous flows, the fluid particles spend a limited time in the mixing zone before leaving the mixer. A study of the residence time distribution of the particles provides a lot of information on the flow behavior [43, 22, 10] and consequently allows to predict the mixing quality. The residence time t_s of a fluid particle inside the mixer is defined as the time it takes to pass through the mixing zone, from the inlet to the outlet. Knowing the position of each particle at each time step as well as the time spent between two consecutive time steps, we calculated the time each particle takes to pass through the mixer. Then, the residence time distribution of the 1000 particles initially

distributed along the inlet section is evaluated.

Chaotic flows are characterized by an exponential divergence of the trajectories [35, 14, 31, 23]. The divergence of the trajectories of two successive particles, initially located next to each other, is calculated. The initial distance l_0 between two successive particles is equal to $l_0 = \frac{W}{1000} = 2.10^{-5}$ m. The distance between two particles at an instant t, l(t), is considered as the Euclidean distance between these two divergent particles. The averaged divergence $\overline{l(t)}$ is computed using the 1000 divergence curves l(t) obtained; see Sec. 3.1.4.

We have noticed that the divergence of the trajectories is influenced by the presence of the walls. The separation of the particles is exponential during only a finite time which corresponds to a maximum limit of separation. For this purpose, finite size Lyapunov exponents λ_{FSLE}, suitable for transport analysis in confined geometries [5, 6], are calculated according to:

$$\lambda_{FSLE} = \frac{1}{t} \ln\left(\frac{l(t)}{l_0}\right). \tag{2}$$

λ_{FSLE} is calculated for each pair of particles initially located next to each other, using their divergence curve l(t), for $\frac{l(t)}{l_0} = 100$. This is the maximum limit of separation; see Fig. 13. t is the time when $\frac{l(t)}{l_0} = 100$. Then, the averaged value $\overline{\lambda}_{FSLE}$ (over the 1000 values of λ_{FSLE}) and the standard deviation $\sigma(\lambda_{FSLE})$ of the finite size Lyapunov exponents are computed.

A classical quantitative parameter to evaluate the homogeneity of a mixture is the standard deviation of the concentration field. It allows to follow the uniformisation of the scalar field in time and/or space [32, 42, 45]. In this study, to quantify the mixing, we calculated the standard deviation of the dimensionless concentration field C^* on a line located at the exit of the mixing zone (the yellow line in Fig. 4), according to:

$$\sigma(C^*) = \sqrt{\frac{1}{N}\sum_{i=1}^{N}(C_i^* - \overline{C^*})^2}. \tag{3}$$

The dimensionless concentration is calculated as $C^* = \frac{I - I_{min}}{I_{max} - I_{min}}$. I is is the grey level, I_{max} and I_{min} correspond respectively to the maximum and minimum grey level at the beginning of each experimental test. $\overline{C^*}$ is the averaged concentration on the exit line

(the yellow line in Fig. 4). N is the number of data points provided on the exit line. Ideally, the standard deviation of the concentration decreases from 0.5 when the two fluids are separated to 0 when the two fluids are perfectly mixed.

3. Results

3.1. Characterisation of the chaotic advection regime

In the present study, two parametric studies are performed. The first one consists in studying the influence of the Strouhal number St on the generation of the chaotic advection regime. To this end, we proceed by varying the period of rotation of the cylinders, given that the speed at the inlet of the mixer does not change. In the second study, we study the influence of the velocity ratio k on the degree of chaos by varying the amplitude of the rotational speed of the cylinders.

3.1.1. Flow topologies

We present in Fig. 5 the velocity fields at different times of the period of rotation of the cylinders, for St = 0.4 and k = 10. The flow topologies are repeated in an identical way at each period since the rotational motions of the cylinders are periodic.

At $t = T$, $T + \frac{T}{2}$ and $2T$ (see Figs. 5(a), 5(c) and 5(e)), the rotational speed of the cylinders goes through zero and the flow velocity is minimal. The velocity vectors are parallel to the channel walls. The velocity is larger at the center of the channel and decreases as it approaches the walls. The velocity field is influenced by the presence of cylinders. The velocity of the flow is larger in the mixing zone where the cross-sectional area becomes narrower because of the protrusion of the cylinders in the channel.

The flow topologies that correspond to the first and second half of the period are similar to those observed in Figs. 5(b) and 5(d) respectively. The velocities are larger or smaller depending on the rotational speed of the cylinders, which reaches its maximum at $t = \frac{T}{4}$ and $t = \frac{3T}{4}$.

During the first half of the period, the cylinders positioned on the same wall rotate counter-clockwise while the opposite cylinder rotates in the opposite direction; see Fig.

5(b). Three vortex structures, located next to the cylinders, are formed. These zones act as a barrier to mass transport and reduce the flow cross-section. We observe that the flow is accelerated in the area between these three recirculation regions.

At the end of the first phase, the elliptical regions, present during the first half of the period, disappear. During the second half of the period, the cylinders change their directions of rotation; see Fig. 5(d). Three new recirculation zones are generated. They are separated from the cylinders and cover almost the entire width of the channel except small areas near the cylinders that allow the flow to pass around the elliptical regions. Back flows are also observed in Fig. 5(d), indicating that the fluid elements are folded during the second half of the period.

The flow topologies, observed in Fig. 5, are schematically illustrated in Fig. 6. Different features of chaotic flow are observed. Parabolic points represented by blue dots appear at the walls. They are due to the non-slip conditions [21]. The flow goes from the unstable parabolic points to the stable parabolic points following the separatrices represented by the blue lines in Fig. 6. During the first half of the period, $T < t < T + T/2$, three elliptical zones appear next to the cylinders within the limit of the separatrices. A part of the fluid particles travel between these zones and are directly advected to the outlet of the mixing zone without being recirculated. At the end of the first half of the period, the three vortices disappear and three new vortices detached from the cylinders appear during the second half of the period, $T + T/2 < t < 2T$. A hyperbolic point is observed and represented by a green square in Fig. 6(b). The central flow follows the unstable direction (represented by the black arrows coming out from the hyperbolic point), passes behind the elliptical zone, then follows the stable direction of the hyperbolic point (represented by the black arrows going to the hyperbolic point) and exits the channel. These two topologies alternate between each other since the motion of the cylinders is periodic. During the switch from the topology 6(a) to the topology 6(b) the separation lines and the elliptical zones, which form barriers to the mass transport, are destroyed, the flow streamlines intersect and mixing occurs. These two flow topologies are completely consistent with the one observed in the numerical study presented in Ref. [18].

By varying St for a fixed k, the flow topologies are similar to those observed in Fig.

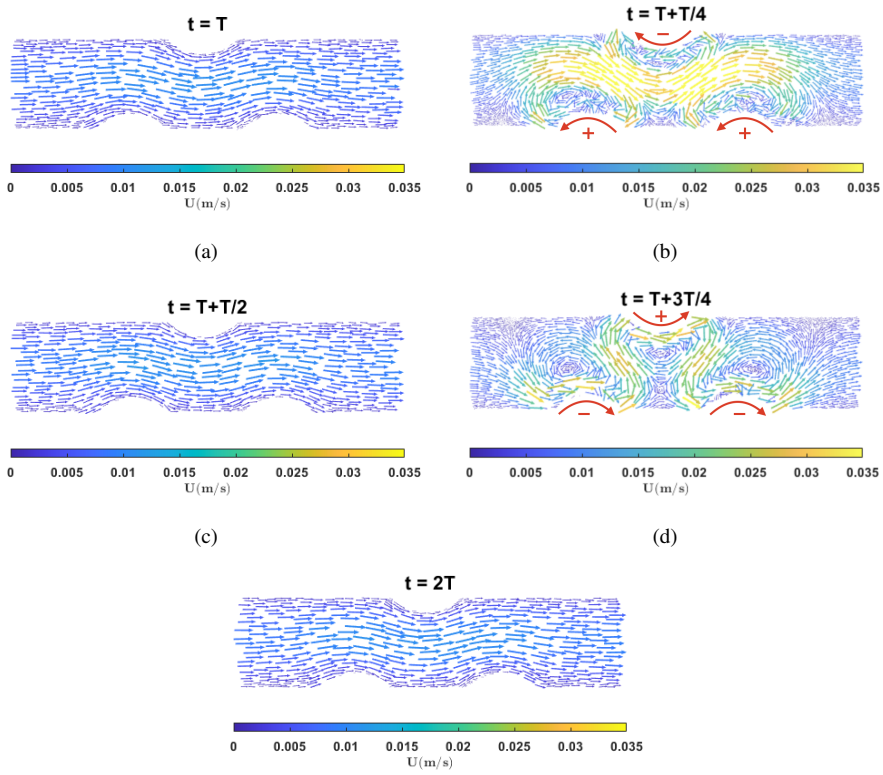

Figure 5: Velocity fields measured by the PIV technique at different times of the period of rotation of the cylinders, (a) t = T, (b) $t = T + \frac{T}{4}$, (c) $t = T + \frac{T}{2}$, (d) $t = T + \frac{3T}{4}$ (e) t = 2T, of a Newtonian fluid flow for St = 0.4 and k = 10. The velocity scale is the same for each figure and evolve from low velocity (dark blue color) to high velocity (yellow color).

6. Since the flow velocity at the inlet is constant, only the duration of each phase differs between two cases realized with two different St. For example, we can observe in Fig. 7 that the velocity fields measured for St = 0.1 and k = 10 are identical to those observed in Fig. 5 for St = 0.4 and k = 10. However, for St = 0.1, the flow evolves slowly from the first to the second topology, because the rotational period of the cylinders (T = 20 s) is longer than the one corresponding to the flow realized with St = 0.4 (T = 5 s).

By varying k for a fixed St, the flow topologies observed during the first and second half of the period are identical to those observed in Fig. 6. However, the velocities are

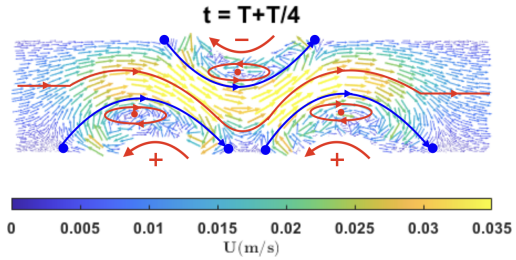

(a) $nT < t < nT + T/2$

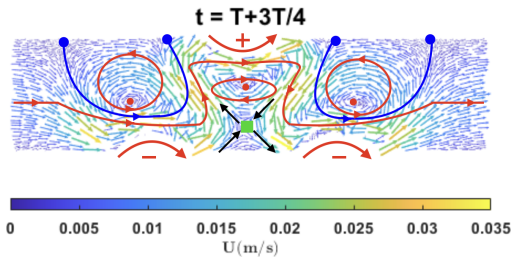

(b) $nT + T/2 < t < (n+1)T$

Figure 6: Topologies of the fluid flow that correspond to the (a) first and (b) second half of the cylinder rotational period. The different symbols correspond to the parabolic points (●), elliptical points (●) and hyperbolic point (■).

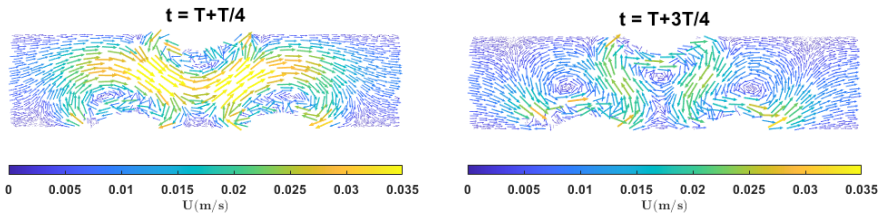

(a) (b)

Figure 7: Velocity fields of a Newtonian fluid flow for St = 0.1 and k = 10 at (a) $t = T + \frac{T}{4}$, (b) $t = T + \frac{3T}{4}$.

more or less important depending on the value of k. For example, we can observe in Fig. 8 that the velocities, for St = 0.4 and k = 15, are larger than those observed in Fig. 5 for k = 10 and for the same value of St, especially in the mixing zone which is the most influenced by the rotational movement of the cylinders.

From the velocity field measurements presented in this section, we can conclude

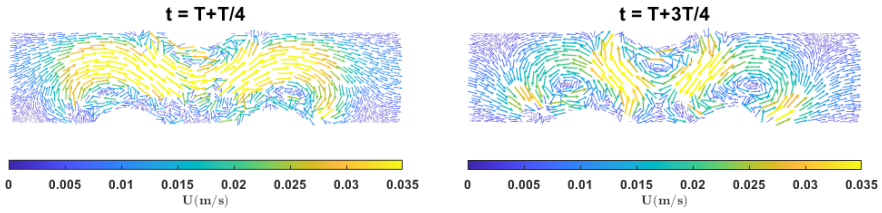

(a) (b)

Figure 8: Velocity fields of a Newtonian fluid flow for St = 0.4 and k = 15 at (a) $t = T + \frac{T}{4}$, (b) $t = T + \frac{3T}{4}$.

that for any given Strouhal number St and velocity ratio k, the flow patterns remain the same: the fluid elements are strongly recirculated in the elliptical regions near the cylinders during the first half of the period and they are folded during the second half of the period.

3.1.2. Influence of the Strouhal number on the chaotic flow

To study the influence of the Strouhal number St on the generation of complex flows, experiments with Emkarox flows are conducted at fixed Re = 0.1, k = 10 and we varied the value of the Strouhal number St between 0.1 and 2, which corresponds to a rotational period of the cylinders between 20 s and 1 s respectively. The advection time $t_a = \frac{L}{U}$ corresponding to this flow is equal to 5.5 s. The trajectories of 1000 particles initially distributed along the inlet section of the mixing zone are computed for the several cases using the method described in Sec. 2.3.4. For visibility reasons, we present in Fig. 9 the trajectories of 30 particles with 10 particles located close to the wall (blue trajectories), 10 particles in the middle of the channel (black trajectories) and 10 particles close to the other wall (red trajectories). The residence time distributions corresponding to the different cases and calculated according to the method described in Sec. 2.3.4, are presented in Fig. 10.

For St = 0.1, the fluid particles have not been trapped by the recirculations, formed next to the cylinders, during the first half of the period. They are accelerated for a sufficiently long time equal to half period of rotation of the cylinders ($\frac{T}{2}$ = 10 s). This time is longer than the characteristic advection time of this flow. Most of the particles

leave the channel during the first half of the period and a first peak is observed on the residence time distribution for St = 0.1 and k = 10; see Fig. 10. We can observe in Fig. 9(a) that the red particles next to the wall and the black particles in the middle exit the channel without being subjected to the stretching and folding process caused by the motion of the cylinders and thus may contribute to a bad mixing detected at the channel exit. The remaining particles are trapped by the recirculations induced by the bottom right side cylinder during the second half of the period. The residence time distribution shows that no particles exit the channel between t = 10 s and t = 20 s. The blue trajectories show recirculations. We deduce then that the fluid elements are subjected to the stretching and folding process during this time ($\frac{T}{2}$ = 10 s) and that the mixing is better during the second half of the period. The cylinders change their direction of rotation again, and the particles are accelerated again and leave the channel during the second period and a second peak is observed on the residence time distribution. The two observed peaks are almost equidistant from the average residence time represented in Fig. 10 by the blue dotted line.

For St = 2, the rotational period of the cylinders, T = 1 s, is very short compared to the advection time. The displacement of the cylinders during a half period ($\Omega_0 \frac{T}{2}$) is very small. Therefore, the flow is not sufficiently influenced by the motion of the cylinders. The transverse displacement of the flow is very small, the fluid elements are not folded and chaotic trajectories are not generated; see Fig. 9(h). Moreover, the residence time distribution observed in Fig. 10 for St = 2 and k = 10 is similar to that of a Poiseuille flow, which confirms that the flow is not chaotic and that mixing is not efficient for this set of parameters.

For intermediate values of the Strouhal number, $0.2 < St < 1$, we can observe the generation of more complex trajectories. If we consider, for example, St = 0.4 (T = 5 s), the fluid elements are accelerated during $0 < t < \frac{T}{2}$ and then folded and trapped by the recirculation zones during the period $\frac{T}{2} < t < T$. During the first period, the fluid particles remain in the channel (no particles leave the channel for t < 5 s; see Fig. 10) because the acceleration time is not enough to allow the particles to exit as for St = 0.1. During the first half of the second period, $T < t < T + \frac{T}{2}$, the flow is accelerated again. The particles that have already crossed further leave the channel and a first peak around

t = 7.5 s is observed in the residence time distribution; see Fig. 10. For $T + \frac{T}{2} < t < 2T$, the remaining particles are trapped by the recirculation zones. For $2T < t < T + 2T + \frac{T}{2}$, the flow is again accelerated and a second peak around t = 12.5 s is observed in the residence time distribution. The remaining particles are recirculated for $2T + \frac{T}{2} < t < 3T$ and most of the particles leave the channel during the first half of the third period which generates a third peak around t = 17.5 s.

We can observe that for intermediate St, the residence time distribution is more homogeneous. The residence times are centered around the average value (the blue dotted line). The tail of distribution is shorter. This means that most of the particles left the mixer at instants close to the average time, so the particles are relatively subjected in the same way to the stretching and folding mechanism. The cylinders change the direction of rotation several times when particles are present in the mixing zone. The fluid elements are stretched and folded several times before leaving the mixer. We can also notice that for the intermediate St, the first peak appears later. This indicates that the particles remain in the mixer for longer time, which can induce better mixing.

We can conclude that, to ensure good mixing, the fluid particles must spend more time in the mixing zone and the cylinders must change the direction of rotation several times so that the fluid elements are sufficiently stretched and folded. This is done by using intermediate values of the Strouhal number. For small values of the Strouhal number, the flow approaches the stationary case, because the rotational period becomes very long. The flow crosses the mixing zone before the cylinders change direction of rotation. For large values of the Strouhal number, the displacement of the cylinders during a half period is small as well as the transverse displacement of the flow. Therefore, it is preferable to use intermediate St to ensure good mixing.

3.1.3. Influence of the velocity ratio k *on the chaotic flow*

To study the influence of the velocity ratio k on the generation of complex flows, experiments with Emkarox flows are conducted at fixed Re = 0.1, St = 0.4 (an intermediate Strouhal number exhibiting chaotic trajectories) and we varied the velocity ratio k.

Fig. 11 shows the trajectories obtained for three different values of k, k = 5, k = 10

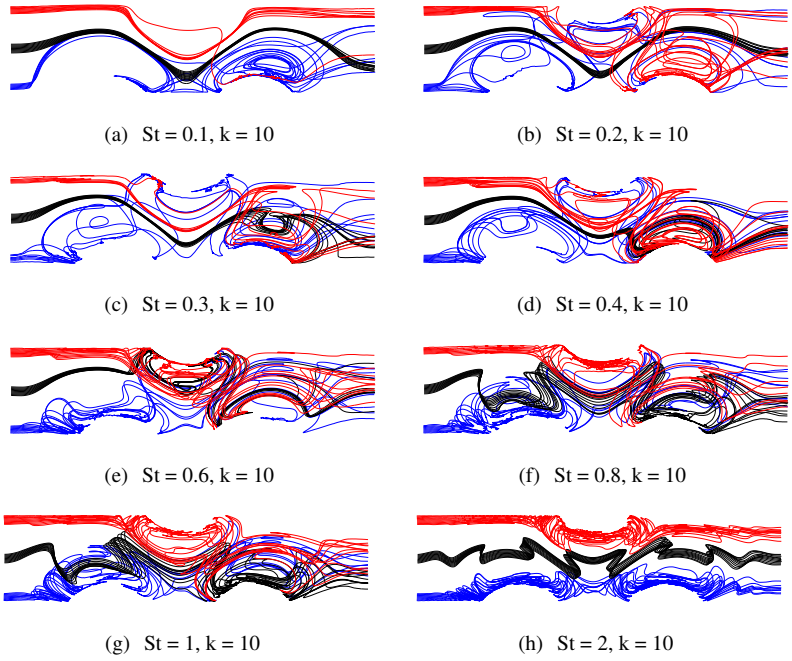

(a) St = 0.1, k = 10 (b) St = 0.2, k = 10

(c) St = 0.3, k = 10 (d) St = 0.4, k = 10

(e) St = 0.6, k = 10 (f) St = 0.8, k = 10

(g) St = 1, k = 10 (h) St = 2, k = 10

Figure 9: Trajectories of 30 particles of a Newtonian fluid flow for k = 10 and different values of St.

and k = 15. For k = 5, the cylinders make fewer turns as the fluid passes through the mixing zone. For this case as well, as for large St, the displacement of the cylinders during half period ($\Omega_0 \frac{T}{2}$) is very small. The trajectories observed in Fig. 11(a) do not show recirculation, the trajectories remain rather parallel to each other especially the blue trajectories positioned next to the wall and the black trajectories positioned in the middle. We can conclude that, for k = 5, the fluid elements are not subjected to the stretching and folding process which results in poor mixing.

The trajectories and the residence time distribution observed for k = 15 are relatively similar to those observed for k = 10 (see Figs. 11 and 12). The maximum time required for the fluid particles to exit the channel is larger for k = 15; see Fig. 12. For higher values of k, the cylinders make more cycles. The fluid particles make more turns in the recirculation zones, the black trajectories in Fig. 11(c) reveal more recirculations. Thus, better mixing can be expected for larger velocity ratio k.

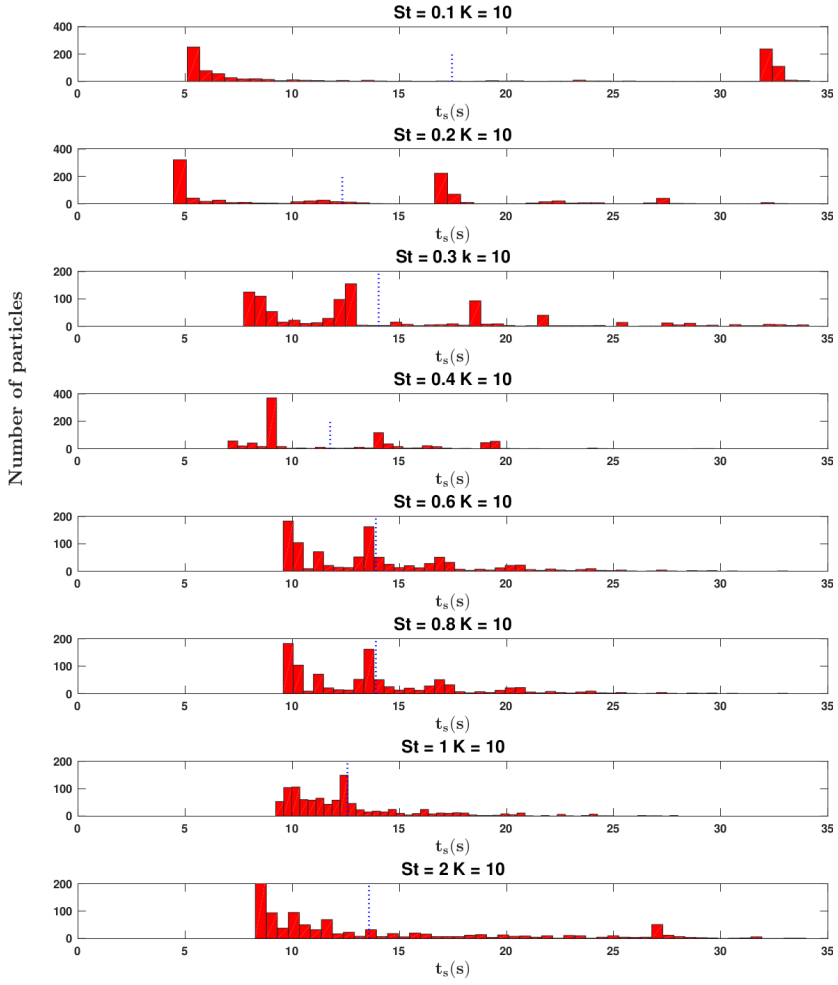

Figure 10: Residence time distribution of 1000 particles of a Newtonian fluid flow for k = 10 and different values of St. The blue dotted vertical line represents the average residence time calculated for 1000 particles. The vertical coordinate is the number of particles exiting the mixer at different time instants.

3.1.4. Quantification of the chaotic advection regime

In order to quantify the chaotic advection regime, we calculated the divergence of the trajectories for each pair of particles located next to each other. Fig. 13 shows the temporal evolution of the averaged divergence of the trajectories, computed according to the method described in Sec. 2.3.4, for some cases previously discussed. For the

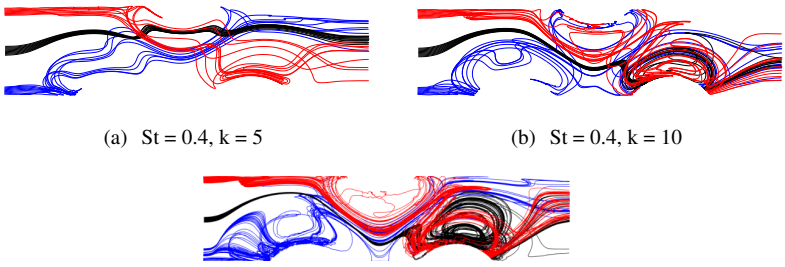

(a) St = 0.4, k = 5 (b) St = 0.4, k = 10

(c) St = 0.4, k = 15

Figure 11: Trajectories of 30 particles of a Newtonian fluid flow for St = 0.4 and different values of k.

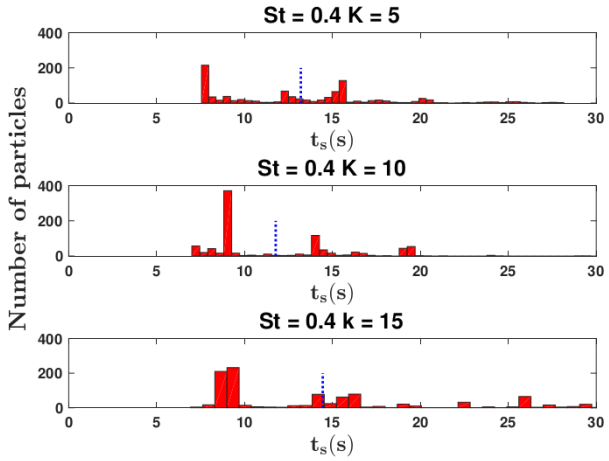

Figure 12: Residence time distribution of 1000 particles of a Newtonian fluid flow for St = 0.4 and different k. The blue dotted vertical line represents the average residence time calculated for 1000 particles. The vertical coordinate is the number of particles exiting the mixer at different time instants.

different sets of parameters (St, k), we can see that the divergence of the trajectories is exponential over a finite time after which the separation of the particles reaches a maximum value due to the presence of the walls. Fig. 13 shows that the maximum separation $\frac{\overline{l(t)}}{l_0}$ is approximately equal to 100. The static curve, shown in Fig. 13, which corresponds to the case where the cylinders do not rotate, never reaches this separation limit.

Since the divergence of the trajectories reaches a maximum limit during a finite

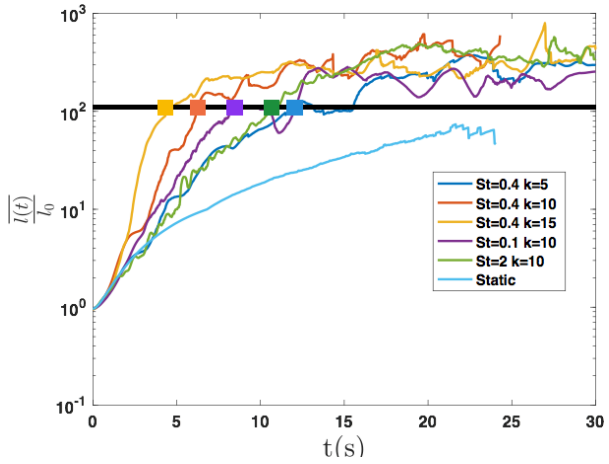

Figure 13: Time evolution of the averaged divergence of trajectories of a Newtonian fluid flow for different values of (St, k).

time, we used the finite size Lyapunov exponents λ_{FSLE} as a parameter to quantify the degree of chaos. It is defined as the inverse of the time needed for the trajectories divergence to reach a certain value. The averages $\overline{\lambda}_{\mathrm{FSLE}}$ and the standard deviations $\sigma(\lambda_{\mathrm{FSLE}})$ of the finite size Lyapunov exponents, computed according to the method described in Sec. 2.3.4, are given in the table 1. The trajectories, for fixed St (St = 0.4), diverge faster when k is larger; see Fig. 13. The average Lyapunov exponent $\overline{\lambda}_{\mathrm{FSLE}}$, observed in table 1, is larger for k = 15. This indicates that the flow is more chaotic for larger velocity ratio k. The standard deviation $\sigma(\lambda_{\mathrm{FSLE}})$ is also larger for k = 15 indicating that the trajectories diverge differently and the particles do not follow the same path.

The trajectories, in the cases with k fixed and equal to 10, and different St, diverge faster for St = 0.4 while the divergence is slower for St = 0.1 and St = 2. Larger $\overline{\lambda}_{\mathrm{FSLE}}$ and $\sigma(\lambda_{\mathrm{FSLE}})$ are observed for St = 0.4. This confirms that the flow is more chaotic for an intermediate Strouhal number.

We can also observe in Fig. 13 that the divergence curve for St = 2 and k = 10 overlaps with the one obtained for St = 0.4 and k = 5. For St = 2, the period of rotation is too short, and for k = 5 the amplitude of rotation speed of the cylinders Ω_0 is too low.

In both cases, the displacement of the cylinders during a half period ($\Omega_0 \frac{T}{2}$) is small and the flow is not sufficiently influenced by the perturbation generated by the cylinders; see Figs. 9(h) and 11(a).

	$\overline{\lambda}_{FSLE}$	$\sigma(\lambda_{FSLE})$
St = 0.4 k = 5	0.4894	0.2310
St = 0.4 k = 10	0.7018	0.2736
St = 0.4 k = 15	1,0126	0.4818
St = 0.1 k = 10	0.5440	0.2458
St = 2 k = 10	0.5491	0.2294

Table 1: Averaged values (calculated for 1000 pairs of particles) and standard deviations of the finite-size Lyapunov exponents for different sets of parameters (St, k).

These observations confirm that the flow is more chaotic for larger velocity ratio k and for an intermediate Strouhal number St in the range of parameters studied.

3.2. Characterisation of the mixing

After studying the influence of the Strouhal number St and the velocity ratio k on the chaotic advection regime, we study in this section the influence of these parameters on the mixing.

3.2.1. Influence of the Strouhal number on the scalar patterns

We first present the study performed with Emkarox flows at Re = 0.1, k = 10 and several values of St. Figs. 14(a), 14(b) and 14(c) show the mixing patterns for St = 0.2, St = 0.4 and St = 1 respectively. For these cases, we distinguish two different mixing patterns. The first one corresponds to the first half of the period. The lower cylinders rotate counter-clockwise and the opposite cylinder rotates in the opposite direction. We notice the presence of three elliptical islands next to the cylinders. In these areas, the fluid elements are strongly recirculated and the striations are formed. Between these regions, the flow is accelerated as observed previously in Fig. 5(b) and the fluid escapes downstream without undergoing the stretching and folding mechanism.The second flow pattern corresponds to the second half of the period. The cylinders change

their directions of rotation and the fluid elements are folded. The two mixing patterns, observed during the first and second half of the period are consistent with the results of the numerical simulations presented in Ref. [18].

For St = 0.2, the flow is accelerated for a very long time (equal to $\frac{T}{2}$), and the fluid escapes the channel. Unmixed regions are detected at the channel outlet during the first half of the period; see Fig. 14(a). As the cylinders change direction of rotation, the fluid elements are folded and gradually exit the channel. Thick striations are observed at the exit because the flow is not sufficiently subjected to the stretching and folding mechanism, which results in a degradation of the mixing quality.

For St = 0.4, the mixing seems more homogeneous; see Fig. 14(b). The number of filaments is larger and their thickness is reduced. The rotational period is not too long and the fluid elements spend more time in the mixing zone between the cylinders and undergo the stretching and folding process several times which contributes to an improvement in the mixing quality.

For St = 1, the elliptical regions are not detected. The rotation period is short (T = 2 s) and the displacement of the cylinders during a half period is small. The flow is not sufficiently influenced by the rotational motion of the cylinders. Poor mixing is observed at the channel outlet. The transversal flow is not large enough to fold the fluid elements and to enhance the mixing. These observations are consistent with the numerical simulations presented in Ref. [18], where it was shown that mixing becomes less favorable for larger Strouhal number.

3.2.2. Influence of the velocity ratio k *on the scalar patterns*

To study the influence of the velocity ratio k on mixing, we fixed the Strouhal number at St = 0.4 for several values of k. The mixing patterns for k = 5, k = 10 and k = 15 are shown in Figs. 15(a), 15(b) and 15(c) respectively. Since the experiments are performed with the same inlet velocity, only the magnitude of the rotational speed of the cylinders differs between these experiments. For larger velocity ratio k, the cylinders make more complete revolutions when the fluid elements are present in the mixing zone. Consequently, finer striations are generated for k = 15 and the mixing is more homogeneous than that observed for k = 5 or k = 10; see Fig. 15. For k = 5,

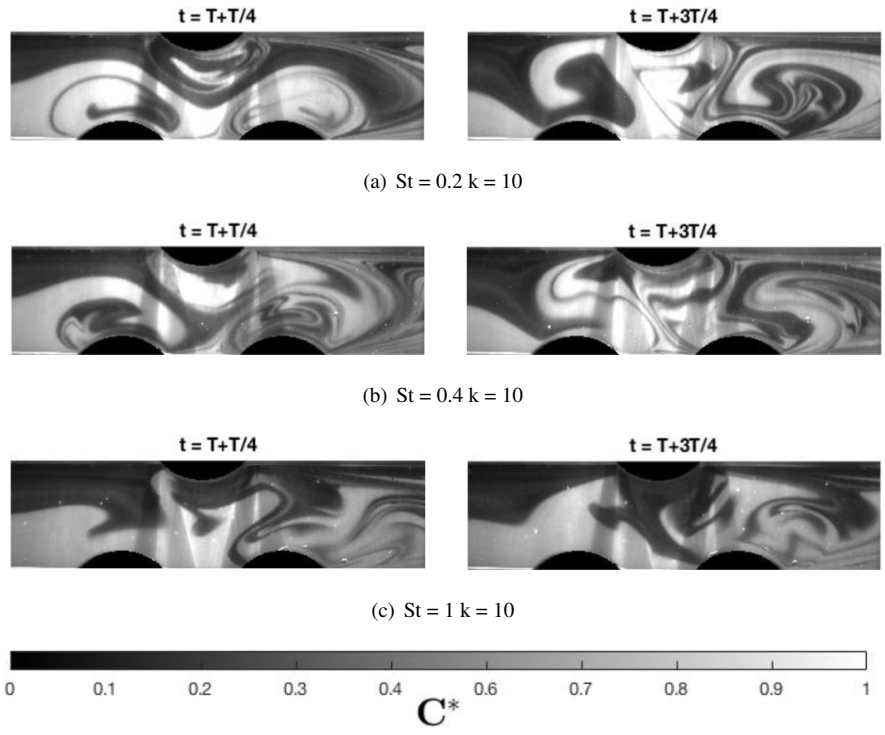

Figure 14: Mixing patterns of a Newtonian fluid flow, for k = 10 and several values of St, at two different times.

the cylinders make fewer cycles as the fluid travels through the mixing zone, so that the flow is less influenced by the rotational motion of the cylinders which results in poor mixing. Thus, better mixing is observed for a higher velocity ratio k. These observations were also noticed from the results of the numerical simulations presented in Ref. [18].

The mixing patterns presented in this section, for several set of parameters (St, k), are completely consistent with the trajectory and the residence time distribution analysis presented in Sec. 3.1.2 and Sec. 3.1.3, and with the quantification of the chaotic advection regime presented in Sec. 3.1.4.

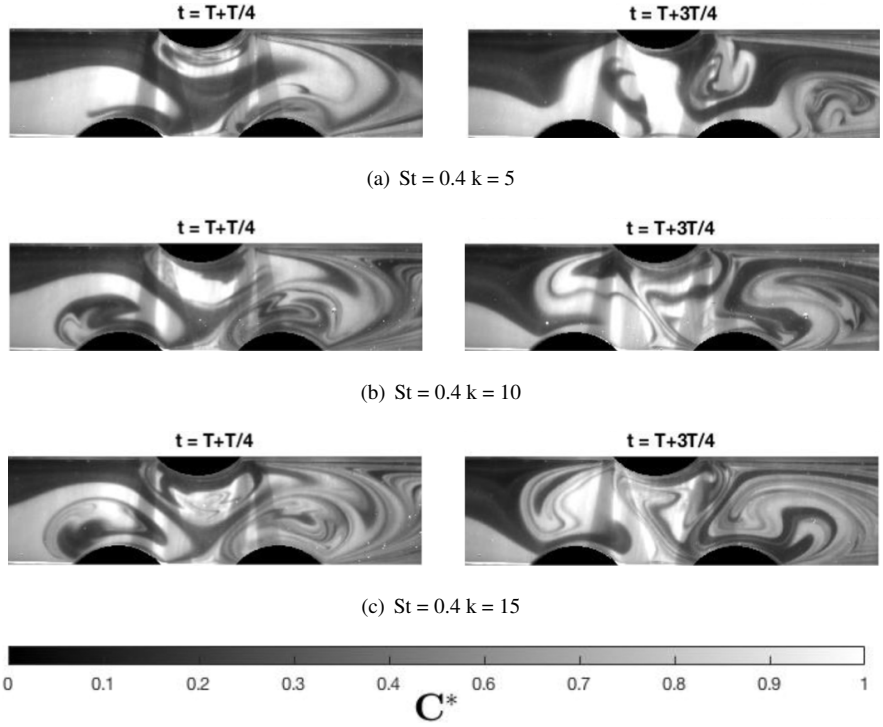

(a) St = 0.4 k = 5

(b) St = 0.4 k = 10

(c) St = 0.4 k = 15

Figure 15: Mixing patterns of a Newtonian fluid flow, for St = 0.4 and several values of k, at two different times.

3.2.3. Quantification of the mixing

In order to quantify the mixing, we computed the temporal evolution of the standard deviation of the concentration field at the exit of the mixer for the different cases we studied, according to the method described in Sec. 2.3.4. Fig. 16 shows the temporal evolution of the standard deviation of the concentration field $\sigma(C^*)$ for the experiments performed at fixed velocity ratio k = 10 and several values of St. Fig. 17 shows the temporal evolution of $\sigma(C^*)$ for the experiments performed at fixed St = 0.4 and several k.

Because of the periodic oscillatory motion of the cylinders, the standard deviations of the concentration oscillate around a mean value with a characteristic frequency equal to that of the rotational frequency of the cylinders. Table 2 shows the mean values of $\sigma(C^*)$, averaged over the last 5 periods, $\overline{\sigma(C^*)}$, and their levels of fluctuation $\sigma(\sigma(C^*))$.

Better mixing quality is observed in Fig. 16 for St = 0.4 since the time-averaged value of the standard deviation of the concentration field is lower compared to the values obtained for St = 0.2 and St = 1; see Table 2. The standard deviation that corresponds to St = 0.2, observed in Fig. 16, shows higher level of fluctuations induced by the concentration gradients. For St = 0.2, the rotational period is too long, the fluid exits the mixer without being sufficiently stretched and folded. For St = 1, the characteristics of chaotic advection are not observed, leading to a poor mixing and a higher value of the mean standard deviation of the concentration field.

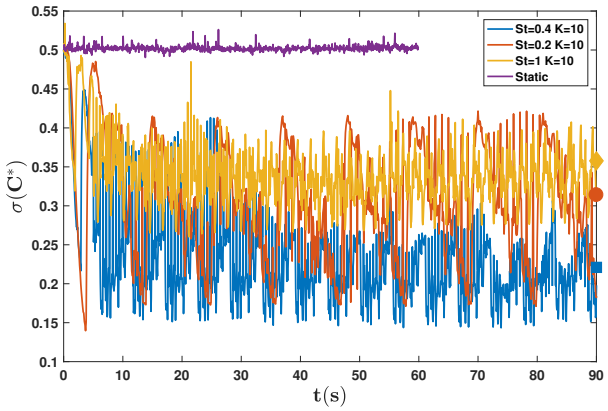

Figure 16: Time evolution of the standard deviation of the concentration field measured at the exit of the mixing zone for several values of St and fixed k = 10. The symbols refer to mean value of the standard deviation of the concentration field of the corresponding case.

Fig. 17 shows that the mixing is more homogeneous for larger k. The cylinders make more revolutions during the presence of the particles in the mixing zone and the generated striations are thinner which promotes the mixing. Therefore, smaller value of $\overline{\sigma(C^*)}$ is observed for larger k; see table 2.

To ensure the best mixing, the time-averaged value of the standard deviation of the concentration field should be as small as possible. The level of fluctuations of the standard deviation of the concentration around the mean also needs to be small so that the resulting mixing can remain homogeneous over time. This is ensured for intermediate Strouhal numbers St and high velocity ratios k.

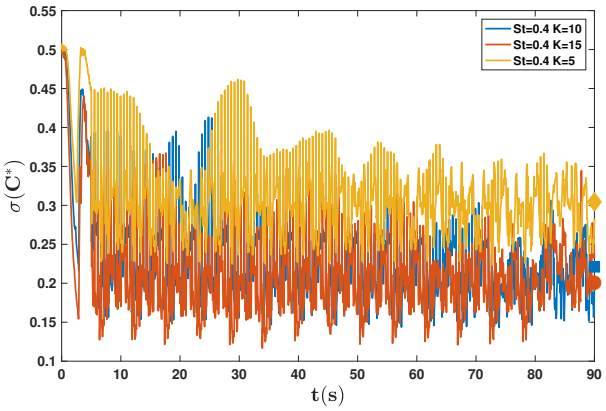

Figure 17: Time evolution of the standard deviation of the concentration field measured at the exit of the mixing zone for several values of k and fixed St = 0.4. The symbols refer to mean value of the standard deviation of the concentration field of the corresponding case.

A good qualitative agreement is noticed between the experimental results and the numerical simulations presented in Ref. [18] where we have shown the existence of an optimal Strouhal number and the possibility to improve the mixing level by adjusting the value of the velocity ratio k.

	$\overline{\sigma(C^*)}$	$\sigma(\sigma(C^*))$
St = 0.2 k = 10	0.3139	0.073
St = 0.4 k = 10	0.221	0.0354
St = 1 k = 10	0.3577	0.0315
St = 0.4 k = 5	0.3045	0.0338
St = 0.4 k = 15	0.2001	0.0319

Table 2: Time-averaged values $\overline{\sigma(C^*)}$ and standard deviations $\sigma(\sigma(C^*))$ of the standard deviation of the concentration field for different values (St, k).

4. Summary and outlook

An experimental study of Newtonian fluid flow at low Re is conducted to highlight the role of different parameters controlling the chaotic mixing induced in a continu-

ous mixer with three rotating cylinders. The parameters controlling the flow are the Strouhal number and the velocity ratio k of the transversal to the axial velocity of the flow. The influence of these parameters on the chaotic mixing is studied using different approaches: trajectory analysis, residence time distribution analysis, finite size Lyapunov exponents, analysis of mixing patterns and standard deviation of the concentration field. We conclude that, in order to achieve good mixing in open flows, the fluid elements must reside within the mixing zone as long as possible so that they undergo sufficient stretching and folding. This conclusion has been also reached by another study of mixing in open flows [21]. To achieve this goal, there exist several alternatives. First, the period of rotation of the cylinders could be decreased in order to increase the number of the stretching and folding operations of the fluid elements while they are in the mixing zone. But the period must not be too small so that the movement of the cylinders can generate sufficient cross flow to fold the fluid elements. Second, the rotational speed of the cylinders could be increased so that the fluid particles are more recirculated while they are in the elliptical regions. However, this can lead to the degradation of the product due to excessive stirring and an increase in the price of the final product to compensate for the additional energy consumption. It would be interesting to estimate in future work the additional energy required when the rotational speed of the cylinders is increased. Last, the mean inlet flow rate could be decreased so that the fluid spends more time in the mixer. However, in a continuous open mixer, where flow rate directly controls the productivity, it is often undesirable to reduce it too much.

This experimental study also served to validate the theoretical and numerical study presented in Ref. [18]. After a systematic characterisation of the chaotic mixing generated in the RAW mixer, several future works could be considered. Future experiments could focus on studying the dependence of the chaotic mixing on the Reynolds number. From a practical perspective, it would be interesting to study the efficiency of the RAW mixer in mixing non-Newtonian fluids (e.g. shear thinning and/or yield stress fluids) which are commonly encountered in a variety of industrial settings.

Acknowledgments

We acknowledge the Agence Nationale de la Recherche (ANR) for the financial support via project NaiMYS (ANR-16-CE06-0003).

We thank Julien Aubril and Gwenael Boitteau from Laboratoire de Thermique et Énergie de Nantes for their help in setting up the experiment.

*

Appendix A. Qualitative comparison between the experimental results and the numerical simulation results

In our previous numerical work [18], we studied the behavior of this mixer for a wide range of parameters (Re, K, St). However, when carrying out the experimental study presented here, it was not possible to perform an experiment that exactly reproduces one of the numerically studied mixing configurations. In order to be able to present a comparison between numerical and experimental results under exactly the same conditions, we present here a complementary numerical study which concerns a mixing configuration studied experimentally.

In the numerical study, the Reynolds number studied was equal to 1, while the experimental requirements led us to study a Re = 0.1 in the present work. It has been shown in [49] that below Re = 1, the Reynolds number of the bulk flow has no effect on the flow. Thus, the trends observed by the two studies remain comparable.

The configuration presented is as follows: Re = 0.1, St = 1 and K = 10. The numerical method used is the one presented in the reference [18] (same numerical schemes, geometry, mesh, time step, etc.). However, it should be kept in mind that the numerical simulation is two-dimensional, while the experiment is three-dimensional.

The numerical and the experimental mixing patterns are presented in Fig. A.18 at 5 different and equidistant times within one period. As it can be seen, these results are quite similar to each other. We can see the same patterns forming in each period. The few differences can be attributed to the slightly different experimental conditions compared to the numerical study, such as the presence of the walls in the third direction

of space (3D flow) as well as an imperfect contact zone between the rotating cylinders and the fixed walls.

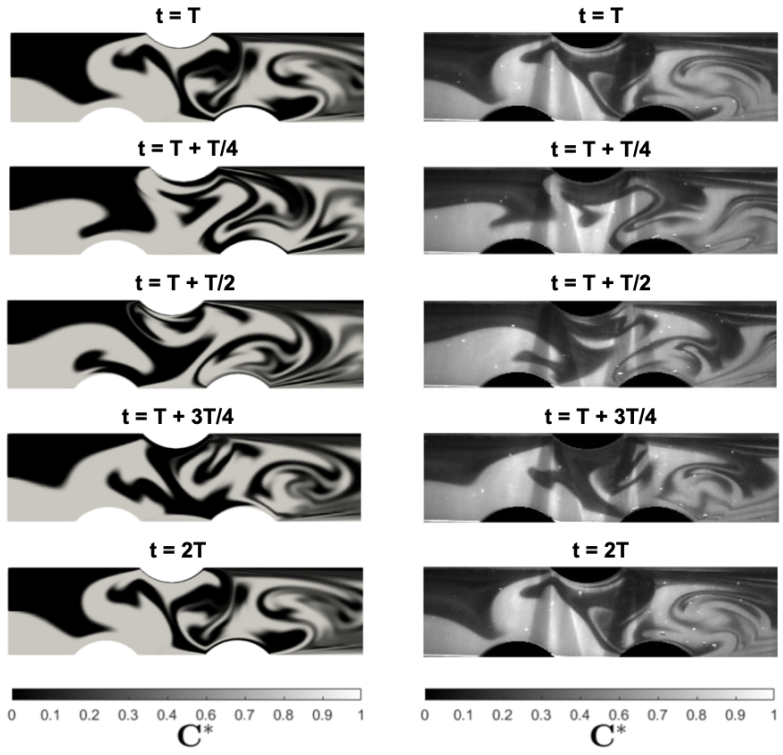

(a) (b)

Figure A.18: (a) Numerical and (b) experimental mixing patterns of a Newtonian fluid flow for Re = 0.1, St = 1 and k = 10 at different times of the period of rotation of the cylinders.

References

[1] N. Acharya, M. Sen, and C. Hsueh-Chia. Heat transfer enhancement in coiled tubes by chaotic mixing. *International Journal of Heat and Mass Transfer*, 35(10):2475–2489, 1992.

[2] F. Aloui, F. Rehimi, E. Dumont, and J. Legrand. Inverse method applied for the determination of the wall shear rate in a scraped surface heat exchanger using the

electrochemical technique. *International Journal of Electrochemical Science*, 3, 06 2008.

[3] H. Aref. Stirring by chaotic advection. *Journal of Fluid Mechanics*, 143:1–21, 1984.

[4] H. Aref, J. R. Blake, M. Budišić, S. S. S. Cardoso, J. H. E. Cartwright, H. J. H. Clercx, K. El Omari, U. Feudel, R. Golestanian, E. Gouillart, G. F. van Heijst, T. S. Krasnopolskaya, Y. Le Guer, R. S. MacKay, V. V. Meleshko, G. Metcalfe, I. Mezić, A. P. S. de Moura, O. Piro, M. F. M. Speetjens, R. Sturman, J.-L. Thiffeault, and I. Tuval. Frontiers of chaotic advection. *Reviews of Modern Physics*, 89:025007, Jun 2017.

[5] V. Artale, G. Boffetta, A. Celani, M. Cencini, and A. Vulpiani. Dispersion of passive tracers in closed basins: Beyond the diffusion coefficient. *Physics of Fluids*, 9(11):3162–3171, 1997.

[6] E. Aurell, G. Boffetta, A. Crisanti, G. Paladin, and A. Vulpiani. Predictability in the large: an extension of the concept of Lyapunov exponent. *Journal of Physics A: Mathematical and General*, 30(1):1–26, jan. 1997.

[7] O. Baskan, H. Rajaei, M. F. M. Speetjens, and H. J. H. Clercx. Scalar transport in inline mixers with spatially periodic flows. *Physics of Fluids*, 29(1):013601, 2017.

[8] G. B. Benbelkacem-Benmouffok. *Viscoélasticité et écoulements de fluides structurés*. PhD Thesis, Institut National Polytechnique de Lorraine, 2009.

[9] I. Bendixson. Sur les courbes définies par des équations différentielles. *Acta Mathematica*, 24:1–88, 1901.

[10] C. Castelain, D. Berger, P. Legentilhomme, A. Mokrani, and H. Peerhossaini. Experimental and numerical characterisation of mixing in a steady spatially chaotic flow by means of residence time distribution measurements. *International Journal of Heat and Mass Transfer*, 43(19):3687 – 3700, 2000.

[11] C. Castelain, A. Mokrani, Y. Le Guer, and H. Peerhossaini. Experimental study of chaotic advection regime in a twisted duct flow. *European Journal of Mechanics - B/Fluids*, 20(2):205 – 232, 2001.

[12] C. Castelain, A. Mokrani, P. Legentilhomme, and H. Peerhossaini. Residence time distribution in twisted pipe flows: helically coiled system and chaotic system. *Experiments in Fluids*, 22(5):359–368, 1997.

[13] C. Chagny, C. Castelain, and H. Peerhossaini. Chaotic heat transfer for heat exchanger design and comparison with a regular regime for a large range of Reynolds numbers. *Applied Thermal Engineering*, 20(17):1615–1648, 2000.

[14] A. Crisanti, M. Falcioni, A. Vulpiani, and G. Paladin. Lagrangian chaos: transport, mixing and diffusion in fluids. *La Rivista del Nuovo Cimento (1978-1999)*, 14(12):1–80, 1991.

[15] J. Duplat, C. Innocenti, and E. Villermaux. A nonsequential turbulent mixing process. *Physics of Fluids*, 22(3):035104, 2010.

[16] J. DUPLAT and E. Villermaux. Mixing by random stirring in confined mixtures. *Journal of Fluid Mechanics*, 617:51–86, 2008.

[17] K. El Omari and Y. Le Guer. Alternate rotating walls for thermal chaotic mixing. *International Journal of Heat and Mass Transfer*, 53(1):123 – 134, 2010.

[18] K. El Omari, E. Younes, T. Burghelea, C. Castelain, Y. Moguen, and Y. Le Guer. Active chaotic mixing in a channel with rotating arc-walls. *Physical Review Fluids*, 6:024502, 2021.

[19] E. Fourcade, R. Wadley, H. C. Hoefsloot, A. Green, and P. D. Iedema. CFD calculation of laminar striation thinning in static mixer reactors. *Chemical Engineering Science*, 56(23):6729 – 6741, 2001.

[20] T. Frommelt, M. Kostur, M. Wenzel-Schäfer, P. Talkner, P. Hanggi, and A. Wixforth. Microfluidic mixing via acoustically driven chaotic advection. *Physical Review Letters*, 100:034502, 02 2008.

[21] E. Gouillart. *Chaotic mixing by rod-stirring devices in open and closed flows*. PhD Thesis, Université Pierre et Marie Curie - Paris VI, 2007.

[22] C. Habchi and J.-L. Harion. Residence time distribution and heat transfer in circular pipe fitted with longitudinal rectangular wings. *International Journal of Heat and Mass Transfer*, 74:13 – 24, 2014.

[23] C. Habchi, J.-L. Harion, S. Russeil, D. Bougeard, F. Hachem, and A. Elmarakbi. Chaotic mixing by longitudinal vorticity. *Chemical Engineering Science*, 104:439 – 450, 2013.

[24] S. M. Hosseinalipour, A. Tohidi, M. Shokrpour, and N. M. Nouri. Introduction of a chaotic dough mixer, part a: mathematical modeling and numerical simulation. *Journal of Mechanical Science and Technology*, 27(5):1329–1339, 2013.

[25] S. W. Jones, O. M. Thomas, and H. Aref. Chaotic advection by laminar flow in a twisted pipe. *Journal of Fluid Mechanics*, 209:335–357, 1989.

[26] D. Khakhar, J. Franjione, and J. Ottino. A case study of chaotic mixing in deterministic flows: The partitioned-pipe mixer. *Chemical Engineering Science*, 42(12):2909 – 2926, 1987.

[27] Y. Le Guer and K. El Omari. Chaotic advection for thermal mixing. In *Advances in Applied Mechanics*, volume 45, pages 189–237. Elsevier, 2012.

[28] Y.-K. Lee, J. Deval, P. Tabeling, and C.-M. Ho. Chaotic mixing in electrokinetically and pressure driven micro flows. In *Microreaction technology*, pages 185–191. Springer, 2001.

[29] R. H. Liu, M. A. Stremler, K. V. Sharp, M. G. Olsen, J. G. Santiago, R. J. Adrian, H. Aref, and D. J. Beebe. Passive mixing in a three-dimensional serpentine microchannel. *Journal of Microelectromechanical Systems*, 9(2):190–197, 2000.

[30] H. E. Meijer, M. K. Singh, and P. D. Anderson. On the performance of static mixers: A quantitative comparison. *Progress in Polymer Science*, 37(10):1333 – 1349, 2012. Topical Issue on Polymer Physics.

[31] B. Metzger and J. Butler. Irreversibility and chaos: Role of long-range hydrodynamic interactions in sheared suspensions. *Physical review. E, Statistical, nonlinear, and soft matter physics*, 82:051406, 11 2010.

[32] A. Mokrani, C. Castelain, and H. Peerhossaini. The effects of chaotic advection on heat transfer. *International Journal of Heat and Mass Transfer*, 40(13):3089–3104, 1997.

[33] R. Moussu and F. Pelletier. Sur le théorème de Poincaré-Bendixson. In *Annales de l'Institut Fourier*, volume 24, pages 131–148, 1974.

[34] F. Muzzio, P. Swanson, and J. M. Ottino. The statistics of stretching and stirring in chaotic flows. *Physics of Fluids A: Fluid Dynamics*, 3(5):822–834, 1991.

[35] J. Ottino. Mixing, chaotic advection, and turbulence. *Annual Review of Fluid Mechanics*, 22(1):207–253, 1990.

[36] J. M. Ottino. *The kinematics of mixing: stretching, chaos, and transport*, volume 3. Cambridge university press, 1989.

[37] H. Peerhossaini, C. Castelain, and Y. Le Guer. Heat exchanger design based on chaotic advection. *Experimental Thermal and Fluid Science*, 7(4):333 – 344, 1993.

[38] H. Poincaré. Mémoire sur les courbes définies par une équation différentielle (i). *Journal de Mathématiques Pures et Appliquées*, 7:375–422, 1881.

[39] M. Raffel, C. E. Willert, S. T. Wereley, and J. Kompenhans. *Particle Image Velocimetry: A Practical Guide (Experimental Fluid Mechanics)*. Springer; 2nd edition, September 2007.

[40] F. Raynal and J. Gence. Efficient stirring in planar, time-periodic laminar flows. *Chemical Engineering Science*, 50(4):631 – 640, 1995.

[41] F. Raynal and J.-N. Gence. Energy saving in chaotic laminar mixing. *International Journal of Heat and Mass Transfer*, 40(14):3267 – 3273, 1997.

[42] E. Saatdjian, A. Rodrigo, and J. Mota. Stokes flow heat transfer in an annular, rotating heat exchanger. *Applied Thermal Engineering*, 31(8-9):1499–1507, 2011.

[43] A. K. Saxena and K. D. P. Nigam. Coiled configuration for flow inversion and its effect on residence time distribution. *AIChE Journal*, 30(3):363–368, 1984.

[44] F. Scarano and M. L. Rhiethmuller. Advances in iterative multigrid piv image processing. *Experiments in Fluids*, 29, 2001.

[45] A. D. Stroock and G. J. McGraw. Investigation of the staggered herringbone mixer with a simple analytical model. *Philosophical Transactions: Mathematical, Physical and Engineering Sciences*, 362(1818):971–986, 2004.

[46] B. Timité, C. Castelain, and H. Peerhossaini. Mass transfer and mixing by pulsatile three-dimensional chaotic flow in alternating curved pipes. *International Journal of Heat and Mass Transfer*, 54(17):3933 – 3950, 2011.

[47] B. Timité, M. Jarrahi, C. Castelain, and H. Peerhossaini. Pulsating flow for mixing intensification in a twisted curved pipe. *Journal of Fluids Engineering-transactions of The ASME*, 131, 12 2009.

[48] E. Villermaux and J.-P. Hulin. Lagrangian chaos and mixing of viscous fluids. *European Journal of Physics*, 11:179, 12 2000.

[49] E. Younes. *Nouveau mélangeur à advection chaotique pour les fluides visqueux newtoniens et à seuil*. PhD Thesis, Université de Nantes (UN), 2020.

[50] E. Younes, V. Bertola, C. Castelain, and T. Burghelea. Slippery flows of a carbopol gel in a microchannel. *Physical Review Fluids*, 5:083303, 2020.

[51] J. Zambaux, J. Harion, S. Russeil, and P. Bouvier. Combining two orthogonal secondary flows to enhance the mixing in an annular duct. *Chemical Engineering Research and Design*, 94:702 – 713, 2015.

[52] M. Zsugyel, T. Tél, and J. Józsa. Numerical investigation of chaotic advection past a groyne based on laboratory flow experiment. *Advances in Water Resources*, 71:81 – 92, 2014.